

增材/等材复合制备 Sc/Zr 改性 Al-Mg 合金工艺研究

赵宇辉^{1,2}, 贺晨^{1,2*}, 赵吉宾^{1,2}, 邹健³, 王志国^{1,2}, 何振丰^{1,2}

¹中国科学院沈阳自动化研究所, 辽宁 沈阳 110016;

²中国科学院机器人与智能制造创新研究院, 辽宁 沈阳 110169;

³沈阳航空航天大学机电工程学院, 辽宁 沈阳 110135

摘要 为了实现高性能、低孔隙率 Al-Mg-Sc-Zr 合金在航空航天主承力结构领域的广泛应用,采用激光熔化沉积-热轧复合工艺制备了 Al-Mg-Sc-Zr 合金试样。基于金相显微镜、扫描电子显微镜、显微硬度和室温拉伸实验等检测方法,探究了复合工艺与微观组织和力学性能之间的关系,确定了最优工艺参数;研究了热轧压下量对沉积态试样微观组织演变、微孔缺陷闭合行为及力学性能的影响规律。结果表明:微孔缺陷随压下量的增加而逐渐减少,当压下量达到 50% 时,微孔缺陷完全闭合,试样的强度和硬度显著提高,熔合线区域合金元素的分布变得均匀。在优化的工艺参数条件下,复合工艺制备试样的抗拉强度、屈服强度、延伸率和硬度分别为 412 MPa、243 MPa、22.8% 和 118.76 HV,较未轧制试样分别提高了 22.6%、12.5%、54.1% 和 15.3%。

关键词 材料; Al-Mg-Sc-Zr 合金; 激光熔化沉积; 热轧工艺; 微观组织; 力学性能

中图分类号 TG146 **文献标志码** A

DOI: 10.3788/AOS221673

1 引言

Al-Mg 合金作为最关键的轻质结构材料之一,因其密度低、比强度和刚度,在航空航天领域得到广泛应用^[1-2]。作为一种新型的高强度铝合金,Al-Mg-Sc-Zr 合金具有高弹性模量、高比强度和优异的抗损伤性能^[3]。航空航天制造业的快速发展,对复杂几何形状铝合金结构件提出了更高性能的要求。而增材制造(AM)技术在解决这些问题方面具有显著的优势^[4-6]。

激光增材制造技术按其工艺原理主要分为两大类:1)基于粉末床熔融的激光选区熔化(SLM)技术;2)基于同轴送粉式的激光熔化沉积(LMD)技术。LMD 技术因其具有高设计自由度、高附加值零件原位修复能力、高可靠性及高生产效率等优点,被认为是 21 世纪增材制造业最有发展前景和最可行的技术之一^[7-9]。到目前为止,关键航空装备对高性能铝合金结构件需求的不断增加,推动了锻造型 2000 系^[10]、5000 系^[11]、6000 系^[12]和 7000 系^[13]铝合金增材制造工艺与技术的广泛研究。以往的研究表明,气孔是铝合金增材制造加工过程最典型的冶金缺陷,严重影响增材工件的拉伸力学性能与疲劳性能。

Gu 等^[14]通过轧制将由电弧熔丝增材制造

(WAAM)制备的 AA2219 铝合金的孔隙率降低到 0.05%,从而使其屈服抗拉强度和极限抗拉强度分别提高了 110% 和 22.6%,但伸长率降低了 57%。除了气孔缺陷外,微结构和相变也会通过 WAAM 对铝合金的力学性能产生重大影响。Bai 等^[15]使用钨极气体保护电弧增材制造方法制备了 2219 铝合金试样,随后的热处理有效地改善了其力学性能,这归因于 Al-Cu 共晶的溶解以及时效热处理后 θ' 相的析出。Zhong 等^[16]采用 WAAM 技术生产了薄壁 AA2050 铝合金零件,通过热处理,其显微硬度达到 141 HV,抗拉强度达到了 400 MPa。然而,McPherson 等^[17]和 Toda 等^[18]报道,高温期间产生的热应力可促进微孔的聚集,从而导致微孔的总体积有所增加。Zhou 等^[19]使用 WAAM 制造 AA2219 铝合金,并研究了电弧移动速度对增材工件宏观形貌、微观结构和力学性能的影响规律,结果表明,电弧移动速度设定为 350 mm/min,促进了 θ (Al₂Cu)相、细等轴晶的形成,并获得更高的抗拉强度(273.5 MPa)和屈服强度(182.9 MPa)。Gu 等^[20]研究了采用 WAAM 技术制备的 Al-Cu 合金的微观孔隙率对其力学性能的影响规律,发现该合金具有大量微孔缺陷,并量化了微孔的形态和尺寸分布,热处理后的平均屈服强度和抗拉强度分别增加了 116%

收稿日期: 2022-09-02; 修回日期: 2022-10-22; 录用日期: 2022-11-25; 网络首发日期: 2022-12-10

基金项目: 国家自然科学基金(52105415)、国防科技重点实验室基金(JCKY61420052017)

通信作者: *hechen@sia.cn

和 66%。然而,他们没有给出消除 WAAM 制造中气孔冶金缺陷的解决方案。综上所述,微孔缺陷对合金强度和韧性影响较大^[21]。Al-Mg-Sc-Zr 合金中低熔点的 Mg 元素含量较高,在 LMD 制造过程中更容易蒸发与汽化,以及液态铝中的氢溶解度大约是固态铝在高温下的氢溶解度的 20 倍,最终导致由 LMD 制备的 Al-Mg-Sc-Zr 合金比其他铝合金具有更大的微孔可能性^[22]。因此,了解和分析 LMD 过程中微孔的空间分布、热处理后微孔的演化特征以及抑制微孔的方法,对提高 Al-Mg-Sc-Zr 合金的综合力学性能具有重要意义。

本文研究了利用 LMD 工艺制备的 Al-Mg-Sc-Zr 合金的微孔缺陷形成机制,讨论了热变形过程形变量对 Al-Mg-Sc-Zr 合金微孔缺陷的演变规律,并对沉积试样的微孔形态、分布和力学性能进行了表征与分析。

表 1 Al-Mg-Sc-Zr 合金粉末和基板的化学成分

Table 1 Chemical composition of Al-Mg-Sc-Zr alloy powder and substrate

Element		Mg	Sc	Zr	Mn	Zn	Cu	Fe	Si	Al
Mass fraction / %	Powder	5.87	1.01	0.37	0.54	0.3	0.01	0.1	0.036	Bal.
	Substrate	4.64	0.76	0.27	0.54	0.2	0.01	0.1	0.028	Bal.

如图 1 所示,基于中国科学院沈阳自动化研究所的第四代激光增材制造系统,开展相关激光熔化沉积实验,实验平台包括波长为 1064 nm 的 YLS-10000-KC

此外,提出一种减少 LMD 铝合金微孔、促进沉淀强化的复合方法,以期利用 LMD 技术制备大尺寸、高性能铝合金零件提供一定的工艺参考与数据支撑。

2 实验

2.1 实验材料与方法

本次激光熔化沉积实验采用的材料是由北京有色金属研究总院生产的 Al-Mg-Sc-Zr 合金雾化球形铝合金粉末,粒径范围为 75~150 μm ,粉末的霍尔流动性数值为 87 s/50 g,采用电感耦合等离子体发射光谱仪(ICP-OES 5800)对金属粉末和基板化学成分进行检测,结果如表 1 所示。基板为 $\Phi 110 \text{ mm} \times 20 \text{ mm}$ 尺寸的铸态 Al-Mg-Sc-Zr 合金圆棒,实验开始前用 400# 砂纸打磨以去除基板表面的氧化膜,并用质量分数为 75% 的无水乙醇溶液擦洗。

激光器、kuka 机器人、双桶式载气送粉器、同轴送粉喷嘴,柔性 Ar 气氛保护舱、氧含量分析仪等。

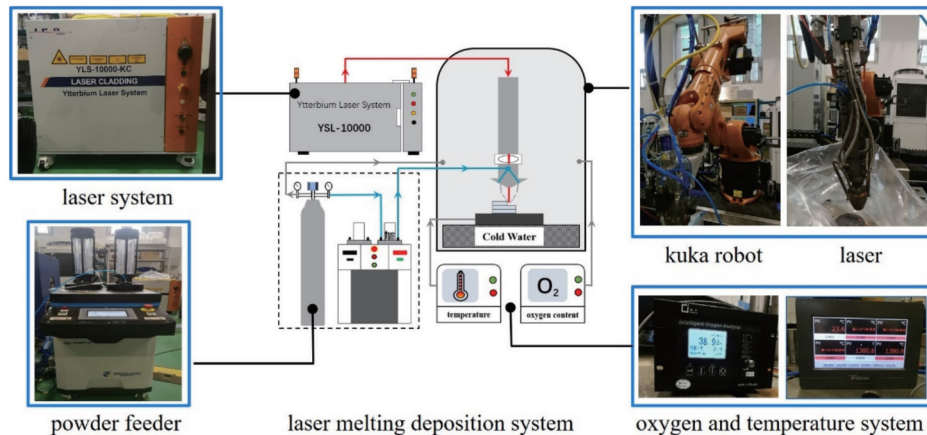


图 1 激光熔化沉积增材制造系统

Fig. 1 Laser melting deposition additive manufacturing system

2.2 样品制备

采用激光熔化沉积技术,制备出 70 mm \times 10 mm \times 40 mm (长 \times 宽 \times 高)的 Al-Mg-Sc-Zr 合金沉积试样,其工艺参数如下:激光功率为 3500 W、扫描速率为 10 mm/s、送粉速率为 0.7 r/min、光斑直径为 4 mm、载气流量为 3.3 L/min、搭接率为 50%、氧的质量分数 $\leq 50 \times 10^{-6}$ 。通过对 LMD 成形 Al-Mg-Sc-Zr 合金的实验研究发现,气孔目前是 LMD 成形 Al-Mg-Sc-Zr 合金最主要的缺陷,也是对 Al-Mg-Sc-Zr 合金沉积试样力学性能影响较大的因素之一。本文通过设计不同的压

下量(15%、30%、50%)热轧实验对沉积体内部的气孔进行后期焊合,对合金试样(图 2)进行强化处理,并分析不同压下量对 LMD 成形 Al-Mg-Sc-Zr 合金的孔隙焊合行为、微观形貌以及力学性能等的影响规律。

对轧制态试样进行线切割取样,经镶嵌、打磨、抛光后通过光学显微镜(Zeiss Axio Observe A1)观察样品截面处微观组织及缺陷情况,分析不同工艺条件对沉积试样致密度的影响规律;使用 FM-310 显微硬度仪检测试样硬度;使用 Keller 试剂(HF: 2 mL; HNO₃: 5 mL; HCl: 3 mL; H₂O: 190 mL)腐蚀样品 30 s 后,使



图 2 不同热轧压下量处理的沉积试样

Fig. 2 Deposited samples treated with different hot rolling reduction drafts

用光学显微镜及扫描电镜观察微观组织,并分析微观组织的演变情况;拉伸试样的取样位置如图 3(a)~(c)所示,尺寸如图 3(d)所示,采用 INSTRON 5982 型万能试验机进行室温拉伸实验,拉伸速率为 1 mm/min。

3 分析与讨论

3.1 轧制工艺对 Al-Mg-Sc-Zr 合金微观组织的影响

不同热轧变形工艺条件下,沉积试样孔隙缺陷的截面形貌如图 4 所示。由图 4 可见,沉积态试样的孔隙缺陷以气孔为主,缺陷较为圆整。随着热轧压下量由

15% 增加至 50%,圆形的孔隙缺陷逐渐扁平化,气孔的闭合与压力大小和受力合金的变形程度有关,气孔缺陷逐渐焊合。当热轧压下量为 50% 时,孔隙缺陷基本消失,获得了几乎全致密的增材试样,与此同时,晶界处的结晶相也开始碎化,尺寸逐渐减小,在“孔隙消除+加工硬化+结晶相细化”复合作用下,沉积试样的综合力学性能显著提升。

图 5 为沉积层内微观组织的高倍 SEM 图像。合金经 15% 压下量轧制处理后,晶粒尺寸变化不大,与低倍 SEM 图像中的气孔变化规律相近。经 30%、50% 压下量轧制处理后,可以从图 5(c)、(d)中观察到晶粒被明显拉长,晶界处共晶相逐渐细化。通过与未经轧制处理的试样对比可发现,当压下量增加到 30% 以上,来自试样顶部垂直方向的压力,即轧制方向的压力将 α -Al 基体及第二相挤压变形,变形程度沿着压下量的增加逐渐增大,当压下量增大到 50% 时,沉积体内部组织发生了严重纤维化。部分第二相在轧制力的作用下发生破碎,被轧碎的第二相分布随着晶粒的形变方向延展。Al-Mg-Sc-Zr 合金在厚度方向上所受变形抗力较小,相对于长度方向,厚度方向的变形为自由变形,因此在沉积试样的厚度方向平面应变变量较大。

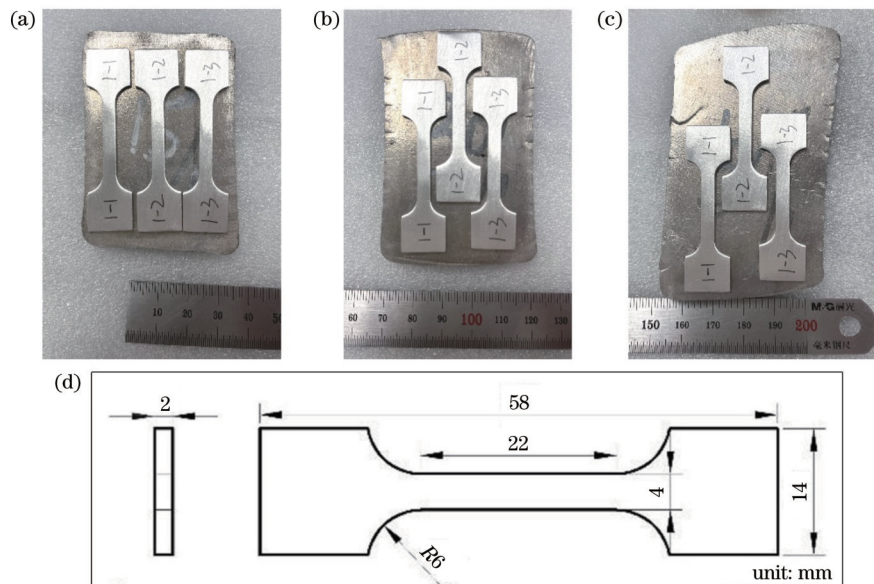


图 3 不同压下量时的拉伸试样取样位置和尺寸。(a) 15%;(b) 30%;(c) 50%;(d) 拉伸试样尺寸

Fig. 3 Sampling position and size of tensile specimen with different reduction drafts. (a) 15%; (b) 30%; (c) 50%; (d) size of tensile specimen

如图 6 所示,通过对未轧制试样及压下量为 50% 的沉积试样熔合线位置的线扫描对比可以看出,未轧制试样在熔合线边界位置的 Sc、Zr 含量较高,轧制后的试样熔合线位置的 Sc、Zr 元素分布则更加均匀。这是因为位于熔合线位置的第二相被轧碎后沿着晶粒的形变方向延展分布,随着压下量的增加,晶界被显著拉长,此处聚集的大块状、富含 Sc、Zr 元素的结晶相逐

渐碎化,晶粒尺寸变得细小,导致结晶相细化且分布变得均匀。

3.2 轧制工艺对 Al-Mg-Sc-Zr 合金显微硬度的影响

如图 7 所示,对未轧制,压下量分别为 15%、30%、50% 的沉积试样进行显微硬度分布分析,沿其沉积方向(图 7 白色箭头指示方向)平行取三列,每列 10~15 个点进行显微硬度测试,载荷为 1.96 N,加载时间为 15 s。

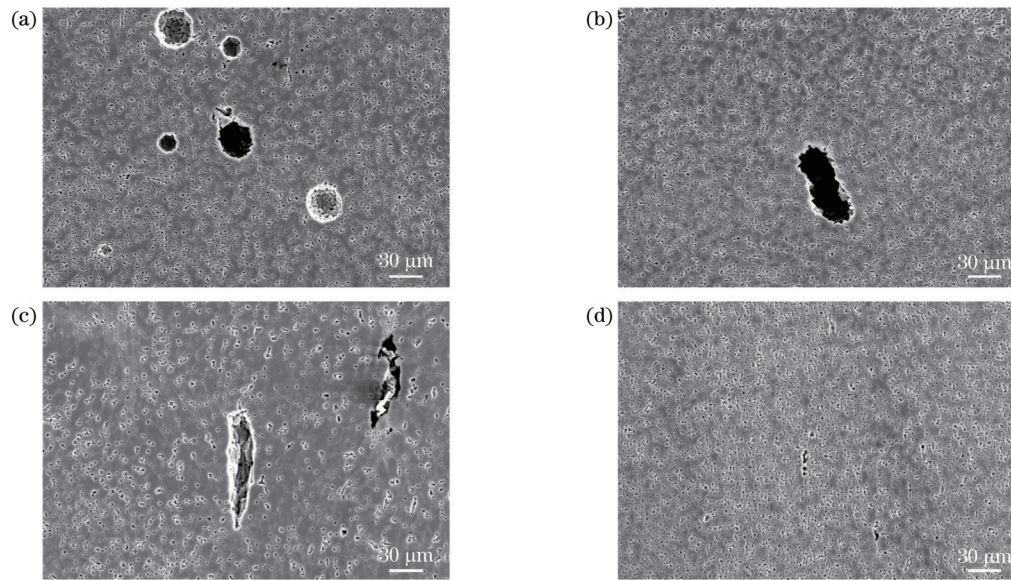


图 4 不同压下量时沉积试样内部横截面的 SEM 图像。(a) 0%; (b) 15%; (c) 30%; (d) 50%

Fig. 4 SEM images of deposited samples with different reduction drafts. (a) 0%; (b) 15%; (c) 30%; (d) 50%

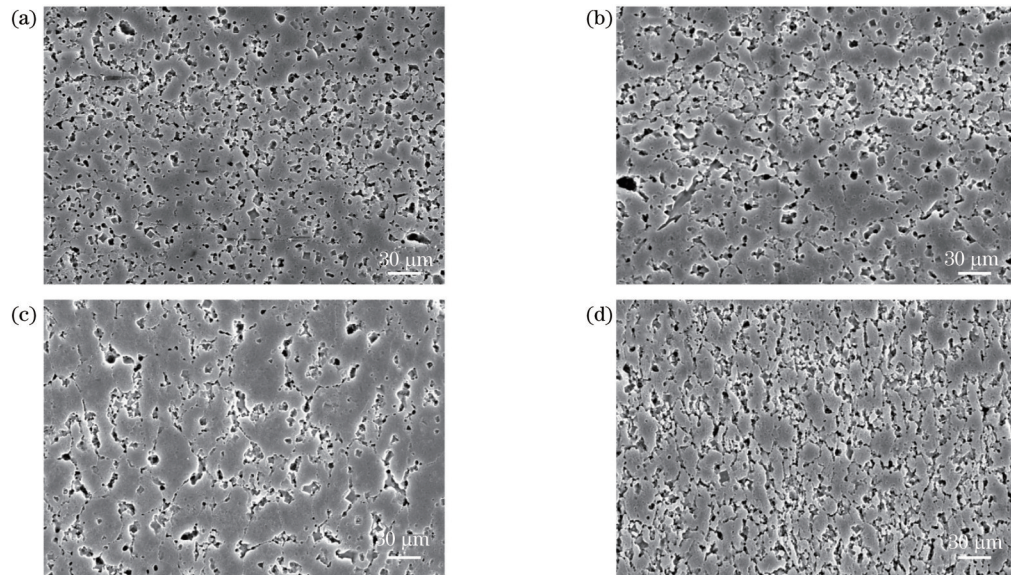


图 5 不同压下量时沉积层内等轴晶粒的 SEM 微观形貌。(a) 0%; (b) 15%; (c) 30%; (d) 50%

Fig. 5 SEM morphologies of equiaxed grains in the deposited layer with different reduction drafts. (a) 0%; (b) 15%; (c) 30%; (d) 50%

显微硬度检测结果如图 8 所示。从图 8 可以看出,对利用 LMD 成形的 Al-Mg-Sc-Zr 合金试样分别按照 15%、30% 和 50% 的压下量进行轧制处理后,显微硬度随压下量的增大呈近似线性提高,但 15% 压下量的沉积试样相较未经轧制处理的沉积试样,显微硬度的提升不明显。未轧制试样的平均硬度值在 $103 \text{ HV}_{0.2}$ 左右,15% 压下量试样的硬度均值在 $106 \text{ HV}_{0.2}$ 左右。而当压下量达到 30% 及以上时,相比前两者,试样的硬度有了明显提升。30% 压下量的试样硬度均值在 $113.64 \text{ HV}_{0.2}$, 50% 压下量的试样硬度均值在 $118.76 \text{ HV}_{0.2}$ 。从图 8(c)、(d) 可以看出,合金试样的硬度开始出现明显的周期性波动,这可能与轧制过程

中的非均匀形变以及应变的累积有关,而且随着压下量的增大,沉积试样的加工硬化效应逐渐增强,从而提高试样的显微硬度值与硬度分布均匀性。

3.3 轧制工艺对 Al-Mg-Sc-Zr 合金力学性能的影响

图 9 所示为未轧制,以及压下量分别为 15%、30% 及 50% 的沉积试样的应力应变曲线,其中图 9(a) 为 50% 压下量时拉伸试样平行段表面宏观形貌,图 9(b) 为未轧制拉伸试样平行段表面宏观形貌。可以看出,未轧制、压下量为 15% 的试样拉伸性能相近,提升效果不明显,而压下量为 30% 及压下量为 50% 的试样拉伸性能较前两者有了大幅提高,其变化趋势与硬度的变化趋势相近。未轧制时试样的抗拉强度、屈服强度

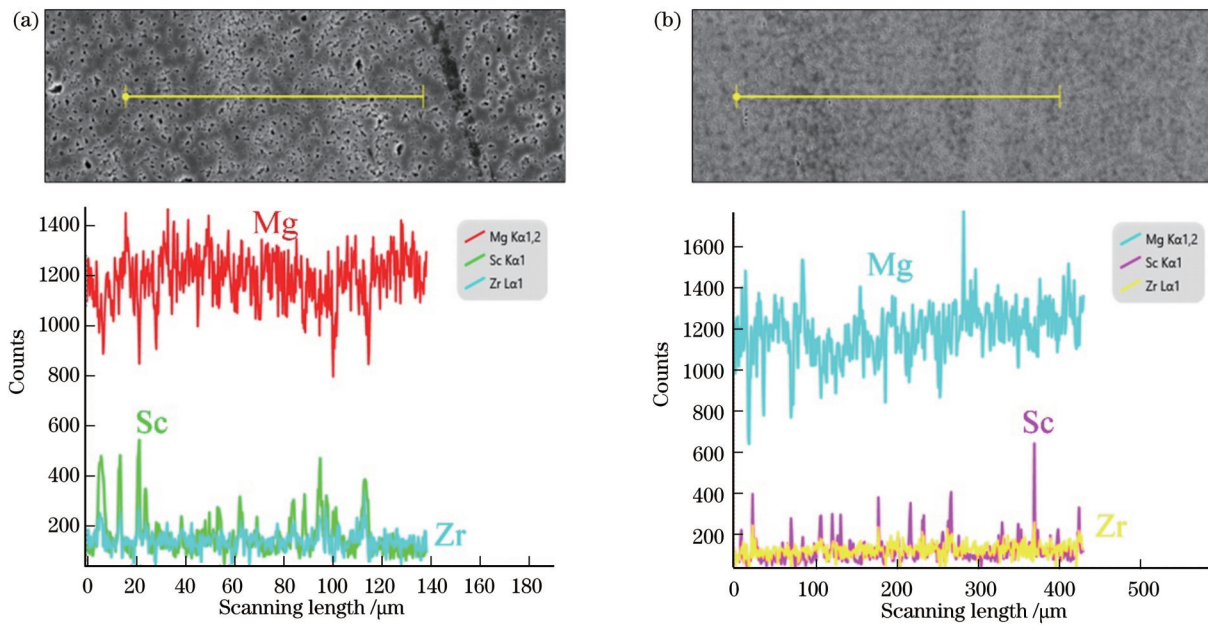


图 6 不同热轧压下量试样熔合线处线扫描结果。(a)未轧制;(b)压下量为 50%

Fig. 6 Line scanning results of fusion line of samples with different hot rolling reduction drafts. (a) Non-rolled; (b) reduction draft of 50%

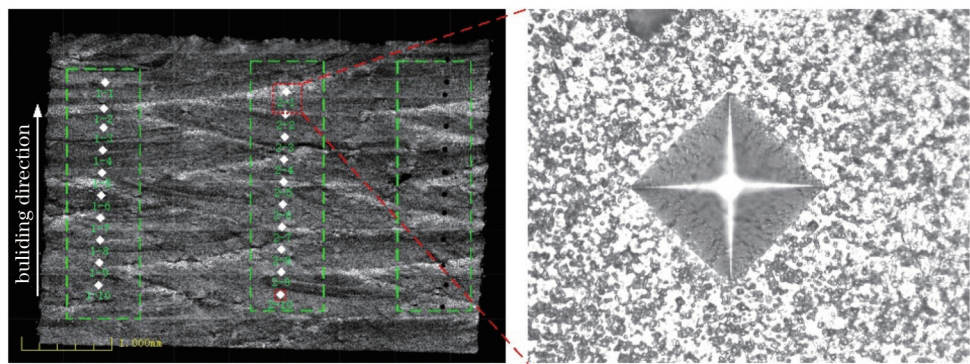


图 7 显微硬度检测打点示意图

Fig. 7 Dot diagram of micro-hardness testing

和延伸率分别为 336 MPa、216 MPa 和 14.8%；当压下量为 50% 时，抗拉强度、屈服强度和延伸率分别为 412 MPa、243 MPa 和 22.8%。合金轧制处理后的抗拉强度和屈服强度均随压下量的增加而呈现线性增长趋势。从图 9 可以发现，15% 压下量试样的拉伸性能提升并不明显，这也说明若想完全消除沉积试样中的气孔缺陷，压下量要达 30% 以上。

轧制后试样强度和硬度提高的主要原因是加工硬化、组织碎化和气孔缺陷消除的综合作用。随着压下量的增加，加工硬化效果逐渐增强，位错密度不断增大，因此位错在运动时的相互交割加剧，即产生固定的位错缠结等障碍，使位错运动的阻力增大，变形抗力增大，塑性变形难度增加，从而提高金属的强度；晶粒细化的原因在于随着轧制力的增大，沉积态的等轴晶粒发生碎化，平均直径逐渐减小，在轧制后形成了大量细小的亚晶粒结构；同时，随着压下量的增加，气孔缺陷

逐渐闭合，从而增大了后续受力过程试样的有效承载面积。因此，高密度位错堆积、细小亚晶数量增加及沉积缺陷消除的综合作用是轧制态 Al-Mg-Sc-Zr 合金强度、硬度提高的主要原因，当压下量为 50% 时试样的力学性能显著提高。

4 结 论

通过激光增材制造与等材热轧变形(LMD-HR)复合工艺制备了不同条件下 Al-Mg-Sc-Zr 合金块体试样，重点研究了热轧压下量对沉积试样孔隙焊合行为、微观组织演变及力学性能的影响规律，并阐明了力学性能提升的综合影响因素，主要结论如下：

1) 热轧辅助激光熔化沉积复合工艺可以显著提高沉积试样的致密度，最终影响增材工件的综合力学性能。当压下量从 15% 增加到 50% 时，随着沉积试样的压下量越来越大，气孔缺陷由圆整形逐渐趋于闭合状

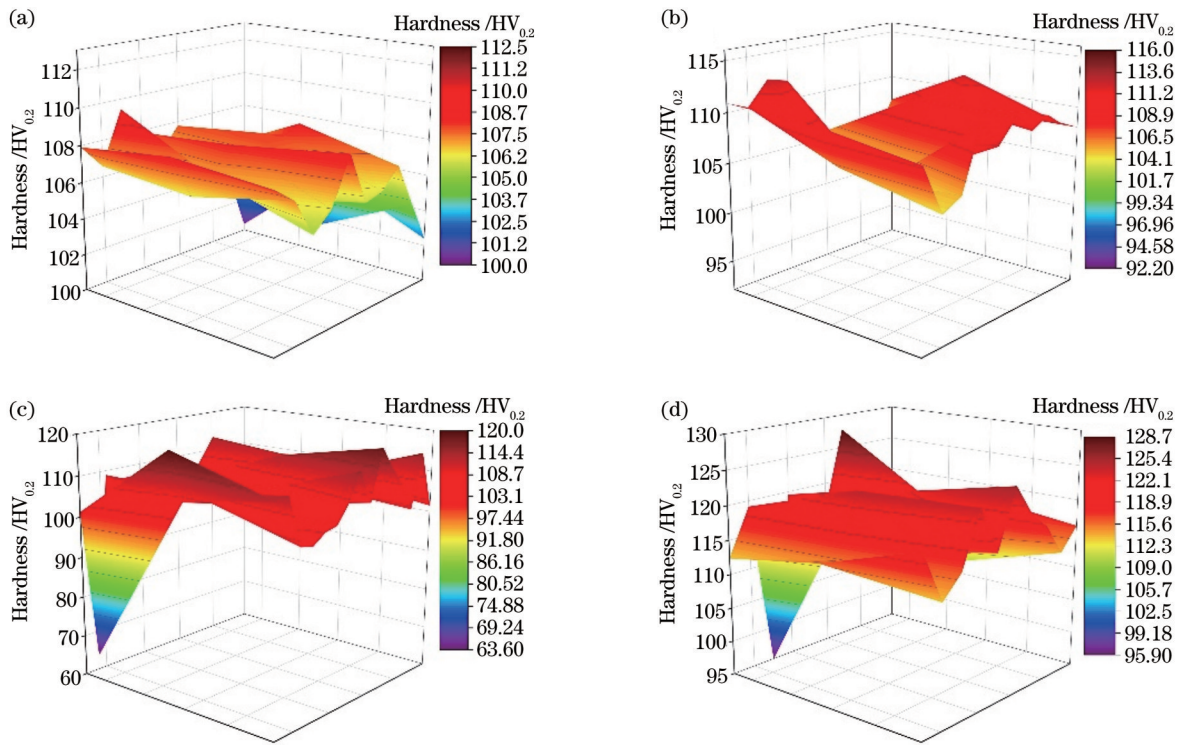


图 8 不同压下量时沉积试样的显微硬度。(a) 0; (b) 15%; (c) 30%; (d) 50%

Fig. 8 Micro-hardness of deposited samples with different reduction drafts. (a) 0; (b) 15%; (c) 30%; (d) 50%

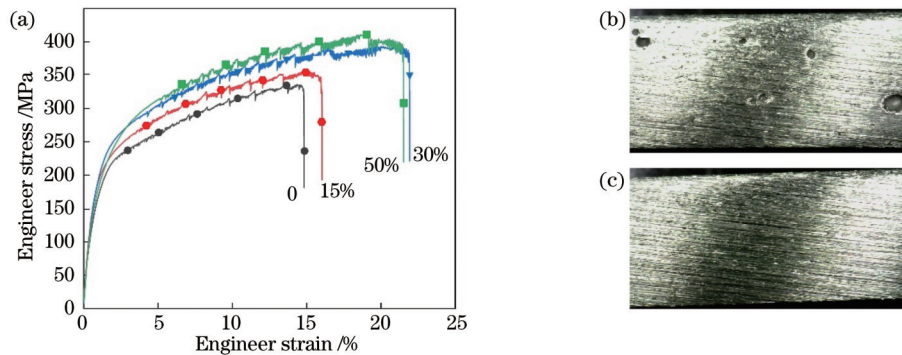


图 9 不同压下量辅助激光熔化沉积试样的应力应变曲线。(a)应力应变曲线;(b)未轧制试样;(c)压下量为 50% 的试样

Fig. 9 Stress-strain curves of laser melting deposition samples with different reduction drafts. (a) Stress-strain curves; (b) non-rolled specimen; (c) specimen with reduction draft of 50%

态。合金的强度和硬度随压下量的增大而线性提高，而且沉积方向硬度分布的均匀性逐渐提高。

2) 基于孔隙缺陷消除、加工硬化与晶粒、晶界处结晶相碎化的协同强化效应，利用复合工艺制备的沉积试样性能明显提高。当热轧压下量为 50% 时，试样的平均显微硬度可达 $(118.76 \pm 2.4) \text{HV}_{0.2}$ ；抗拉强度、屈服强度和延伸率分别由沉积状态下的 336 MPa、216 MPa 和 14.8%，提高到激光熔化沉积/热轧复合制备试样的 412 MPa、243 MPa 和 22.8%，分别提高了 22.6%、12.5% 和 54.1%。

参 考 文 献

[1] 顾冬冬, 张红梅, 陈洪宇, 等. 航空航天高性能金属材料构件

激光增材制造[J]. 中国激光, 2020, 47(5): 0500002.

Gu D D, Zhang H M, Chen H Y, et al. Laser additive manufacturing of high-performance metallic aerospace components[J]. Chinese Journal of Lasers, 2020, 47(5): 0500002.

[2] 秦艳利, 孙博慧, 张昊, 等. 选区激光熔化铝合金及其复合材料在航空航天领域的研究进展[J]. 中国激光, 2021, 48(14): 1402002.

Qin Y L, Sun B H, Zhang H, et al. Development of selective laser melted aluminum alloys and aluminum matrix composites in aerospace field[J]. Chinese Journal of Lasers, 2021, 48(14): 1402002.

[3] 何鹏, 柏兴旺, 周祥曼, 等. MIG 电弧增材制造 6061 铝合金的组织性能[J]. 焊接学报, 2022, 43(2): 50-54, 60, 116.

He P, Bai X W, Zhou X M, et al. Microstructure and properties of 6061 aluminum alloy by MIG wire and arc additive manufacturing[J]. Transactions of the China Welding Institution,

- 2022, 43(2): 50-54, 60, 116.
- [4] Debroy T, Wei H L, Zuback J, et al. Additive manufacturing of metallic components-process, structure and properties[J]. *Progress in Materials Science*, 2018, 92: 112-224.
- [5] Brice C, Shenoy R, Kral M. Precipitation behavior of aluminum alloy 2139 fabricated using additive manufacturing[J]. *Materials Science and Engineering A*, 2015, 648: 9-14.
- [6] Atzeni E, Salmi A. Economics of additive manufacturing for end-use metal parts[J]. *The International Journal of Advanced Manufacturing Technology*, 2012, 62(9): 1147-1155.
- [7] Svetlizky D, Das M, Zheng B, et al. Directed energy deposition (DED) additive manufacturing: physical characteristics, defects, challenges and applications[J]. *Materials Today*, 2021, 49: 271-295.
- [8] Thompson S M, Bian L K, Shamsaei N, et al. An overview of Direct Laser Deposition for additive manufacturing; Part I: transport phenomena, modeling and diagnostics[J]. *Additive Manufacturing*, 2015, 8: 36-62.
- [9] Thompson S M, Bian L K, Shamsaei N, et al. An overview of Direct Laser Deposition for additive manufacturing; Part II: mechanical behavior, process parameter optimization and control [J]. *Additive Manufacturing*, 2015, 8: 12-35.
- [10] 康悦, 赵艳秋, 李悦, 等. 驱动力对 2219 铝合金 DLBSW 焊接熔池行为的影响[J]. *焊接学报*, 2022, 43(2): 82-87, 118.
Kang Y, Zhao Y Q, Li Y, et al. Effect of driving force on molten pool behavior of 2219 aluminum alloy DLBSW process [J]. *Transactions of the China Welding Institution*, 2022, 43(2): 82-87, 118.
- [11] 孙承帅, 张兆栋, 刘黎明. 激光功率对 5356 铝合金激光诱导 MIG 电弧增材制造组织性能的影响[J]. *焊接学报*, 2018, 39(9): 13-18, 129.
Sun C S, Zhang Z D, Liu L M. Effect of laser power on microstructure and properties of 5356 aluminum alloy by laser induced MIG arc additive manufacturing[J]. *Transactions of the China Welding Institution*, 2018, 39(9): 13-18, 129.
- [12] Li R D, Wang M B, Li Z M, et al. Developing a high-strength Al-Mg-Si-Sc-Zr alloy for selective laser melting: crack-inhibiting and multiple strengthening mechanisms[J]. *Acta Materialia*, 2020, 193: 83-98.
- [13] Lei Z L, Bi J, Chen Y B, et al. Effect of energy density on formability, microstructure and micro-hardness of selective laser melted Sc- and Zr- modified 7075 aluminum alloy[J]. *Powder Technology*, 2019, 356: 594-606.
- [14] Gu J L, Ding J, Williams S W, et al. The strengthening effect of inter-layer cold working and post-deposition heat treatment on the additively manufactured Al-6.3Cu alloy[J]. *Materials Science and Engineering A*, 2016, 651: 18-26.
- [15] Bai J Y, Fan C L, Lin S B, et al. Mechanical properties and fracture behaviors of GTA-additive manufactured 2219-Al after an especial heat treatment[J]. *Journal of Materials Engineering and Performance*, 2017, 26(4): 1808-1816.
- [16] Zhong H, Qi B J, Cong B Q, et al. Microstructure and mechanical properties of wire+arc additively manufactured 2050 Al-Li alloy wall deposits[J]. *Chinese Journal of Mechanical Engineering*, 2019, 32(6): 184-190.
- [17] McPherson J W, Dunn C F. A model for stress-induced metal notching and voiding in very large-scale-integrated Al-Si (1%) metallization[J]. *Journal of Vacuum Science & Technology B*, 1987, 5(5): 1321-1325.
- [18] Toda H, Qu P C, Ito S, et al. Formation behaviour of blister in cast aluminium alloy[J]. *International Journal of Cast Metals Research*, 2014, 27(6): 369-377.
- [19] Zhou Y H, Lin X, Kang N, et al. Influence of travel speed on microstructure and mechanical properties of wire+arc additively manufactured 2219 aluminum alloy[J]. *Journal of Materials Science & Technology*, 2020, 37: 143-153.
- [20] Gu J L, Gao M J, Yang S L, et al. Microstructure, defects, and mechanical properties of wire+arc additively manufactured AlCu4.3-Mg1.5 alloy[J]. *Materials & Design*, 2020, 186: 108357.
- [21] Zhang Y B, Xu J, Zhai T, et al. Distributions of pore size and fatigue weak link strength in an A713 sand cast aluminum alloy [J]. *Materials Science and Engineering: A*, 2010, 527(16/17): 3639-3644.
- [22] Boeira A P, Ferreira I L, Garcia A. Alloy composition and metal/mold heat transfer efficiency affecting inverse segregation and porosity of as-cast Al-Cu alloys[J]. *Materials & Design*, 2009, 30(6): 2090-2098.

Process of Sc/Zr-Modified Al-Mg Alloy Prepared by Additive/Equivalent Composite Manufacturing

Zhao Yuhui^{1,2}, He Chen^{1,2*}, Zhao Jibin^{1,2}, Zou Jian³, Wang Zhiguo^{1,2}, He Zhenfeng^{1,2}

¹Shenyang Institute of Automation, Chinese Academy of Sciences, Shenyang 110016, Liaoning, China;

²Institutes for Robotics and Intelligent Manufacturing, Chinese Academy of Sciences, Shenyang 110169, Liaoning, China;

³School of Mechatronics Engineering, Shenyang Aerospace University, Shenyang 110135, Liaoning, China

Abstract

Objective As one of the most important lightweight structural materials, Al-Mg alloy has been widely used in the aerospace field due to its low density, high specific strength, and high stiffness. As a new type of high-strength aluminum alloy, Al-Mg-Sc-Zr alloy offers high elastic modulus, high specific strength, and excellent damage resistance. As the aerospace manufacturing industry develops, higher performance requirements are placed on aluminum alloy structures with complex geometry. Additive manufacturing (AM) technology has significant advantages in solving such problems. This paper is designed to achieve the wide application of high-performance aluminum alloys in primary load-bearing structures in the field of aerospace and obtain additive high-strength Al-Mg-Sc-Zr alloy samples with high compactness

and no porous defects.

Methods The laser melting deposition (LMD) technology is employed to prepare samples with a size of 70 mm×10 mm×40 mm (length×width×height). The processing parameters for the deposited Al-Mg-Sc-Zr alloy samples are a laser power of 3500 W, a scanning rate of 10 mm/s, a powder-feeding rate of 0.7 r/min, a spot diameter of 4 mm, a carrier gas flow rate of 3.3 L/min, an overlap ratio of 50%, and an oxygen mass fraction $\leq 50 \times 10^{-6}$. The experimental study of LMD-processed Al-Mg-Sc-Zr alloy reveals that pores are the most important current defect in this alloy, and it is also one of the factors that greatly affects the mechanical property of the deposited Al-Mg-Sc-Zr alloy samples. In this paper, hot-rolling experiments with different reduction drafts (15%, 30%, and 50%) are conducted to weld the pores in the deposits at a later stage and thereby strengthen the alloy samples. Then, the paper further analyzed the influence of the reduction draft on the pore welding behavior, micromorphology, and mechanical property of the LMD-hot rolling (LMD-HR)-processed Al-Mg-Sc-Zr alloy.

Results and Discussions For the wide application of the Al-Mg-Sc-Zr alloy with high performance and low porosity in primary load-bearing structures in the field of aerospace, Al-Mg-Sc-Zr alloy samples are prepared by the LMD-HR composite process. Metallographic microscopy, scanning electron microscopy, microhardness tests, and tensile tests at room temperature are conducted to explore the relationship of the composite process with microstructure and mechanical property. The optimal process parameters are determined. Then, the paper examines the influence of the hot-rolling reduction draft on the microstructure evolution, microporous defect closure behavior, and mechanical property of the as-deposited samples. The results show that the microporous defects gradually decrease with the increase in the reduction draft. When the reduction draft reaches 50%, the microporous defects are completely closed (Fig. 4). Moreover, the strength and hardness of the sample are significantly improved, and the distribution of alloy elements in the fusion line area becomes uniform. Under the optimized process parameters, the tensile strength, yield strength, elongation, and hardness of the samples prepared by the composite process are 412 MPa, 243 MPa, 23%, and 118.76 HV, respectively, which are 22.6%, 12.5%, 54.1%, and 53.3% higher than those of the unrolled samples, respectively (Fig. 9).

Conclusions In this paper, bulk Al-Mg-Sc-Zr alloy samples are prepared by the LMD-HR composite process under different conditions. The effect of the hot-rolling reduction draft on the pore welding behavior, microstructure evolution, and mechanical property of the deposited samples is emphatically studied. Moreover, comprehensive factors affecting the improvement of mechanical property are clarified. The main conclusions are as follows: the composite process of HR assisting LMD can significantly improve the compactness of the deposited samples, ultimately affecting the comprehensive mechanical property of the additive workpieces. When the reduction is increased from 15% to 50%, the microporous defects tend to close gradually from a round-shape morphology as the reduction draft of the deposited sample increases. The strength and hardness of the alloy increase linearly as the reduction increases, and the hardness distribution in the deposition direction becomes more uniform gradually. Owing to the synergistic strengthening effect of porous defect elimination, work hardening effect, grain fragmentation, and fragmentation of the crystal phase at grain boundaries, the performance of the deposited samples prepared by the composite process is significantly improved. When the hot-rolling reduction draft is 50%, the average microhardness of the samples can reach $(118.76 \pm 2.4) \text{HV}_{0.2}$. The tensile strength, yield strength, and elongation are increased by 22.6%, 12.5%, and 54.1%, respectively, from 336 MPa, 216 MPa, and 14.8% in the deposition state to 412 MPa, 243 MPa, and 22.8% of the samples prepared by the LMD-HR composite process.

Key words materials; Al-Mg-Sc-Zr alloy; laser melting deposition; hot-rolling process; microstructure; mechanical property